Astroparticle Physics 34 (2011) 401–411

Contents lists available at ScienceDirect

Astroparticle Physics

journal homepage: www.elsevier.com/locate/astropart

Corrections for temperature effect for ground-based muon hodoscopes

A.N. Dmitrieva *, R.P. Kokoulin, A.A. Petrukhin, D.A. Timashkov [1]

National Research Nuclear University MEPhI, Moscow 115409, Russia

ARTICLE INFO

Article history:
Received 14 July 2010
Received in revised form 5 October 2010
Accepted 7 October 2010
Available online 31 October 2010

Keywords:
Cosmic ray muons
Temperature effect
Differential temperature coefficients
Muon hodoscopes

ABSTRACT

Influence of atmospheric temperature on muon flux at sea level is considered. Results of calculations of muon spectrum for normal atmospheric conditions, differential temperature coefficients (DTC) for muons at different zenith angles and threshold energies are presented. In calculations, a six-layer stationary spherical model of atmosphere is used, contributions of both pions and kaons as well as dependence of muon energy loss on muon energy are taken into account. Comparison of muon spectrum calculations and experimental data in a wide range of zenith angles and momentums shows a good agreement. Comparison of results of DTC calculations with results of earlier works exhibits only qualitative agreement; possible sources of differences are analyzed. Some practical questions of the use of DTC for muon hodoscope data analysis are discussed.

1. Introduction

Studies of cosmic ray variations at ground level are being carried out more than a half of century [1–4]. The longest series of cosmic ray variation data has been obtained by means of neutron monitors. Several tens of such standardized setups form the global network, which makes it possible to measure variations of intensity and anisotropy of cosmic ray flux. Since neutron monitors are ground-based, in order to analyze extra-atmospheric sources of cosmic ray modulations it is necessary to take into account corrections for the atmospheric effects, mainly for the barometric one [5].

Muon detectors give another possibility for cosmic ray variation investigations [6,7]. The use of muons provides valuable additional opportunities in comparison with neutron monitors: sensitivity to higher energies of primary particles (typical median energies of primary protons for the galactic cosmic ray spectrum for neutron monitors are about 13–16 GeV, for ground based muon detectors about 40–50 GeV), possibility to measure arrival directions of muons and, as a consequence, to study cosmic ray angular variations by means of a single setup.

However analysis of muon intensity variations requires more complicate calculations of the atmospheric corrections taking into account both barometric and temperature effects [5,6]. Besides, unlike neutron monitors, muon detectors are extremely diverse in design and characteristics. One can point out several types of setups used for detection of cosmic ray muons and examination of muon flux variations.

First measurements of variations of penetrating component of cosmic rays (mainly muons) were performed by means of ionization chambers [1,8]. Similarly to neutron monitors, such devices measured only total muon flux from all directions (see [2]). Later, total muon rate variations were also measured by means of scintillation counters [9,10], water Cherenkov detector [11] or proportional wire chambers [12], which were often the elements of setups for extensive air shower detection. In this case, the detectors may have significant area and high counting rate with very low statistical errors.

Along with it, muon telescopes which allow select muons from a given direction of celestial hemisphere began to be used to study cosmic ray variations. Classic muon telescope consists of several charged particle detectors (Geiger–Muller, proportional or scintillation counters) arranged along a straight line and interlaid by an absorbing material: iron, lead, etc. (see [2,13,14]). In some experiments the installation represented a rigid construction which could be rotated in zenith and azimuth direction. For such telescopes the path of the particle in the detector was approximately constant and the setup threshold energy of muons did not depend on zenith angle [15–18]. This fact will be taken into account in the following calculations of temperature coefficients. Drawbacks of classic muon telescopes are low counting rate and lack of ability to detect muons simultaneously from different directions.

Sometimes for analysis of variations of cosmic ray muon flux, data of various detectors with high angular resolution designed for high-energy investigations are used [19–21]. Data acquisition systems of these setups usually permit to detect muons from various directions (as a rule, cosmic ray muons are a background in these setups) but total counting rate of such detectors is not sufficiently high.

* Corresponding author. Tel.: +7 495 323 92 52.
E-mail address: ANDmitriyeva@mephi.ru (A.N. Dmitrieva).
[1] Deceased.

0927-6505/$ - see front matter © 2010 Elsevier B.V. All rights reserved.
doi:10.1016/j.astropartphys.2010.10.013

Multi-directional muon telescopes provide an opportunity to conduct measurements of cosmic ray muon flux variations from different directions of upper hemisphere [22,23]. Such detectors generally consist of two coordinate layers of muon counters and coincidence of signals from the counters in upper and bottom layers separates certain direction of muon arrival. Number of different directions is governed by setup construction and is typically about 10–100. Usually the path of the particle in such detectors increases with increase of zenith angle, so the threshold energy for multi-directional muon telescopes depends on θ. At present, several similar multi-directional muon telescopes are under operation at different points of the globe forming a network for measurements of cosmic ray muon flux variations [24]. Comprehensive review of various types of particle detectors used for cosmic ray variation studies since thirtieth years of XX century can be found in [4].

Construction of muon hodoscopes [25–28] marked the next step in this way and served as a starting point for development of the new direction of distant monitoring of the environment – muon diagnostics [29]. Muon hodoscopes are wide-aperture setups with a high accuracy of individual muon track reconstruction. In contrast to multi-directional muon telescopes, in which detected directions are fixed and their number is limited by discreteness of the setup construction, muon hodoscopes allow register cosmic ray muons and reconstruct muon tracks from practically any direction of upper hemisphere thus measuring continuous angular distribution of muon flux [30]. This ability allows to form muon images of cosmic ray variations at the magnetosphere boundary, which are caused by various disturbances in solar wind and interplanetary magnetic field. However, obtaining of such maps requires a thorough calculation of atmospheric corrections. Threshold energies for muon hodoscopes (as well as for multi-directional muon telescopes) depend on zenith angle. The simplest case is $E_{\min}(\theta) = E_{\min}(0^\circ)/\cos\theta$, and such dependence will be used hereafter. Corrections must be introduced separately for each cell of the angular matrix, besides, simultaneously both for temperature and pressure effects. It requires the development of new methods for such procedures.[2] Earlier calculations aimed at applications for muon telescopes [5,32,33] were performed many years ago. Some of them demand critical re-consideration taking into account contemporary knowledge of parameters of interactions of primary particles and secondary mesons and muons with air, and also appropriate models of the atmosphere. The present work deals with these problems, too.

To introduce corrections for temperature effect, it is necessary to know differential temperature coefficients (DTC) which make it possible to correct counting rate taking into account the changes of the temperature at all altitudes of the atmosphere. And for calculations of barometric effect correction it is necessary to know barometric coefficient $\beta(E_{\min},X,\theta)$ which shows how much the integral muon intensity (or detector counting rate) will be changed if the atmospheric pressure is changed by one pressure unit. With the help of DTC and β it is possible to calculate the corrected intensity N^{corr}:

$$N^{\text{corr}} = N^{\text{obs}} - \Delta N_T - \Delta N_P, \tag{1}$$

where N^{obs} is the experimental muon integral intensity at zenith angle θ, ΔN_T and ΔN_P are atmospheric corrections for changes of atmospheric temperature and pressure.

DTC can be found on the basis of functions describing muon production and propagation in atmosphere.

[2] The same situation takes place for calculations of coupling functions for muon hodoscopes [31].

2. Calculations of muon spectrum

Muon spectrum at the atmospheric depth X may be calculated by using an analytical approach [34]. Meson generation function (by primary cosmic ray particles, neglecting meson regeneration by mesons) may be written as:

$$G^{\eta}(E_\eta, z) = A_\eta \cdot \exp(-z/L_p) \cdot E_\eta^{-\gamma}. \tag{2}$$

Here A_η is the normalization constant ($A_K/A_\pi = 0.15$), E_η is the energy of produced meson (π or K), z is the depth of meson generation along the track (in g/cm^2), L_p is the absorption length of primary nucleons in air, γ is the index of generation function of mesons (index of the differential energy spectrum).

Meson differential spectrum at the depth z taking into account the decay and interaction probabilities will be:

$$J^{\eta}(E_\eta, z, \theta) = \int_0^z dz' G^{\eta}(E_\eta, z') \cdot \exp\left(-\frac{z-z'}{\lambda_\eta} - \frac{l(z)-l(z')}{c\tau_\eta}\cdot\frac{m_\eta c^2}{E_\eta}\right), \tag{3}$$

here λ_η is interaction mean free path of mesons, τ_η is the life-time of mesons ($\tau_\pi = 2.603\cdot10^{-8}$ s, $\tau_K = 1.238\cdot10^{-8}$ s [35]), m_η is the mass of meson ($m_\pi c^2 = 139.6$ MeV, $m_K c^2 = 493.7$ MeV [35]), c is the velocity of light ($c = 2.998\cdot10^8$ m/s), $l(z) - l(z') = \int_{z'}^{z} dy/\rho(y,\theta)$, and $\rho(y,\theta)$ is air density at slant depth y and zenith angle θ (see Fig. 1).

The probability that particle will decay in layer dz equals to $d\tau/\tau$, where $d\tau = dl/c = dz/(\rho(z,\theta)c)$ and $\tau = \tau_\eta E_\eta/(m_\eta c^2)$. So $d\tau/\tau = (m_\eta c^2)dz/(c\tau_\eta\rho(z,\theta)E_\eta)$. For two-body decay in flight, muons are distributed uniformly in energy interval from $(m_\mu/m_\eta)^2 E_\eta$ to E_η and probability that muon energy ε is in the interval dE_η equals to $dE_\eta \Big/ \left(\left(1-(m_\mu/m_\eta)^2\right)E_\eta\right)$. Hence, generation function of muons with energy ε at generation depth z will be:

$$G^{\eta\mu}(\varepsilon, z, \theta) = B_\eta \int_\varepsilon^{(m_\eta/m_\mu)^2\varepsilon} J^{\eta}(E_\eta, z, \theta)\cdot\frac{dE_\eta}{(1-(m_\mu/m_\eta)^2)E_\eta} \cdot\frac{m_\eta c^2}{c\tau_\eta\rho(z,\theta)E_\eta}, \tag{4}$$

here B_η is the probability of two-body $\mu\nu_\mu$ mode of decay ($B_\pi = 1.0, B_K = 0.64$, contributions of other kaon decay modes are neglected), m_μ is the muon mass ($m_\mu c^2 = 105.658$ MeV [35]). Integral is taken over the range of energies which give contribution to muons with energy ε at slant depth z : $(m_\mu/m_\eta)^2 E_\eta \leqslant \varepsilon \leqslant E_\eta$, hence, $\varepsilon \leqslant E_\eta \leqslant (m_\eta/m_\mu)^2\varepsilon$.

So, differential energy spectrum of muons at registration level X and energy E will be:

$$J^{\eta\mu}(E, X, \theta) = \int_0^{z_X} G^{\eta\mu}(\varepsilon(E, z_X - z), z, \theta)\cdot\frac{d\varepsilon(E, z_X - z)}{dE} \cdot\exp\left(-\int_z^{z_X}\frac{m_\mu c^2 dy}{c\tau_\mu\varepsilon(E, z_X - y)\rho(y,\theta)}\right)dz. \tag{5}$$

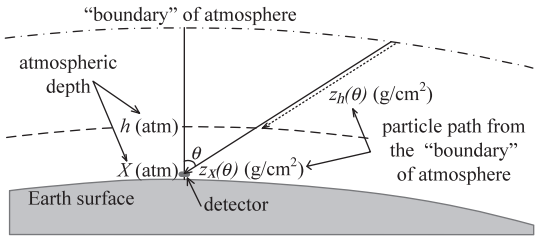

Fig. 1. Scheme for calculations of muon differential spectrum and DTC at atmospheric depth X.

Table 1
Parameters of three temperature profiles of atmosphere: AS, A1 and A2.

Layer, no.	H km	Temperature as a function of altitude $T(H)$, K		
		AS	A1	A2
1	0–11	$288.15 - 6.500 \cdot H$	$298.15 - 6.818 \cdot H$	$262.15 - 5.364 \cdot H$
2	11–25	216.65	223.15	203.15
3	25–46	$216.65 + 2.731 \cdot (H - 25)$	$223.15 + 2.421 \cdot (H - 25)$	$203.15 + 3.374 \cdot (H - 25)$
4	46–54	274	274	274
5	54–80	$274 - 3.423 \cdot (H - 54)$	$274 - 3.423 \cdot (H - 54)$	$274 - 3.423 \cdot (H - 54)$
6	>80	185	185	185

The path z_X along the trajectory of the particle (in g/cm^2) corresponds to the depth X (see Fig. 1). Here additional zenith angle dependence appears since the path of muon from generation point to registration level X depends on θ: it increases with the increase of θ (see Fig. 1). Value τ_μ denotes the life-time of muon ($\tau_\mu = 2.197 \cdot 10^{-6}$ s [35]). Exponential function in (5) takes into account muon decay; this is the probability that muon does not decay and reaches the registration level X. Factor $d\varepsilon/dE$ reflects the change of muon flux because of the energy decrease caused by energy loss.

In expression (5) variable ε (muon energy at slant depth z) is calculated from E (muon energy at registration level X) in a following way:

$$\varepsilon(E, z_X - z) = E - \int_{z_X}^{z} \frac{dE}{dy} dy. \tag{6}$$

For calculation of muon energy loss in air the following formula was used:

$$-\frac{dE}{dz} = a_{\text{ion}}(E, \rho) + b \cdot E. \tag{7}$$

Here $a_{\text{ion}}(E, \rho)$ is ionization loss. Energy losses for bremsstrahlung, pair production, and inelastic interactions of muons in air are approximated by linear function with a constant coefficient $b = 3.27 \cdot 10^{-6}$ cm^2/g. This value of b was obtained from tabulated data for air [36].

Finally, integral intensity of muon flux at the atmospheric depth X:

$$\begin{aligned} N(E_{\min}, X, \theta) &= \int_{E_{\min}}^{\infty} \left(J^{\pi\mu}(E, X, \theta) + J^{K\mu}(E, X, \theta) \right) dE \\ &= \sum_{\eta} \int_{E_{\min}}^{\infty} dE \int_0^{z_X} dz \int_0^{z} dz' \\ &\quad \times \int_{\varepsilon}^{(m_\eta/m_\mu)^2 \varepsilon} dE_\eta F_\eta(E, X, \theta, z, z', E_\eta), \end{aligned} \tag{8}$$

where:

$$\begin{aligned} F_\eta(E, X, \theta, z, z', E_\eta) &= A_\eta \cdot \exp\left(\frac{-z'}{L_p}\right) \cdot E_\eta^{-\gamma} \cdot \frac{B_\eta}{\left(1 - (m_\mu/m_\eta)^2\right) E_\eta} \\ &\quad \cdot \exp\left(-\frac{z - z'}{\lambda_\eta} - \frac{l(z) - l(z')}{c\tau_\eta} \cdot \frac{m_\eta c^2}{E_\eta} \right) \\ &\quad \cdot \frac{m_\eta c^2}{c\tau_\eta \rho(z, \theta) E_\eta} \cdot \frac{d\varepsilon(E, z_X - z)}{dE} \\ &\quad \cdot \exp\left(- \int_z^{z_X} \frac{m_\mu c^2 dy}{c\tau_\mu \varepsilon(E, z_X - y) \rho(y, \theta)} \right). \end{aligned} \tag{9}$$

3. Model of the atmosphere

For muon spectrum calculations, the dependence of air density on altitude above sea level has to be known. In our calculations, a six-layer stationary model of atmosphere [37] was used. The general behavior of the temperature profile is similar to later versions (e.g., US standard atmosphere, 1976); the difference in air temperature does not exceed few degrees at altitudes from 20 to 95 km. In this model, the air is considered as an ideal gas. Dependence of air temperature on altitude above sea level $T(H)$ (see Table 1, AS designation) and molecular mass of dry air $M = 0.02896$ kg/mole are accepted as initial parameters. Ground surface and atmosphere are considered as spherical. Dependence of air pressure and density on altitude H (km) are obtained from the following hydrostatic equations:

$$dP = -\rho(H) g dH = -\frac{M}{R} \cdot \frac{P(H)}{T(H)} dH, \tag{10}$$

here $g = 9.81$ m/s^2 is acceleration of gravity (we neglect here its altitude dependence), $R = 8.314$ J/(mole $\times$ K) is the universal gas constant.

Pressure within each layer $[H_i, H_{i+1}]$ can be calculated by means of following formulas:

$$\int_{P(H_i)}^{P(H)} \frac{dP'}{P'} = -\frac{M \cdot g}{R} \int_{H_i}^{H} \frac{dH'}{T(H')}, \tag{11}$$

$$P(H) = P(H_i) \cdot \exp\left(-\frac{M \cdot g}{R} \int_{H_i}^{H} \frac{dH'}{T(H')} \right), \tag{12}$$

where H_i is the lower boundary of the layer and $P(H_i)$ is the pressure at this altitude.

Dependence of air temperature on altitude above sea level for standard atmosphere is shown in Fig. 2 by solid line (AS designation). In the same figure, real measurements of temperature for Moscow region (Russia) [38] during February (the month of low

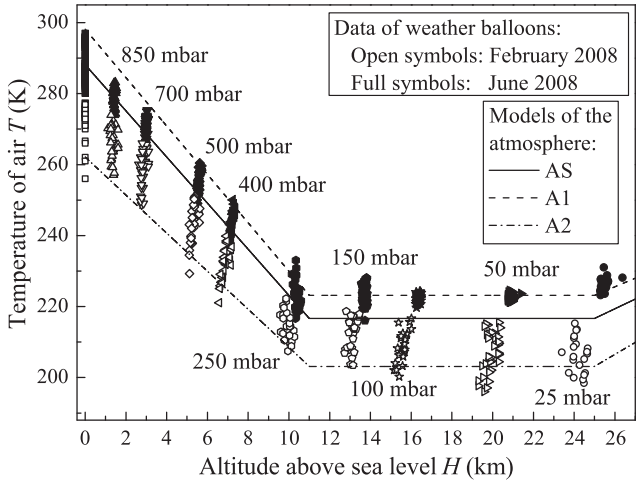

Fig. 2. Dependence of air temperature on altitude above sea level. Balloon measurements (Moscow,Russia) for 2008 are shown by symbols. Different atmosphere models are shown by lines. AS is the standard atmosphere; A1 and A2 are additional profiles.

temperatures) and during June (the month of high temperatures) of 2008 are shown by open and full symbols, respectively. Weather balloons are launched twice a day, and for several pressure levels (925, 850, 700 mbar and others) the altitude above sea level and temperature of air are measured. One can see from the figure that the difference between summer and winter days may reach about 40 K.

For various estimations presented below, additional profiles of the atmosphere A1 and A2 were introduced in a following way. For each of them new values of parameters were defined (see Table 1) in order that the whole range of air temperatures during all the year was covered. Pressure and density of air for these profiles were calculated similar to the standard by formulae (12). Temperature profiles A1 and A2 are shown by additional lines in Fig. 2.

4. Comparison of muon spectrum calculations with experimental data

Results of muon spectrum calculations for standard atmosphere and comparison with experimental data are presented in following figures.

In Fig. 3, calculated muon spectrum for zenith angle $\theta = 0°$ is compared with magnetic spectrometer experimental data (Nottingham [39], Kiel [40], Okayama [18], CAPRICE 94 [41], L3+C [42]). For convenience of comparison the intensities are multiplied by cube of momentum. In our calculations, the following values of parameters were used: $\gamma = 2.7$, $L_p = 110$ g/cm^2, $\lambda_\pi = 120$ g/cm^2 and $\lambda_K = 150$ g/cm^2 (solid line in Fig. 3). Normalization $A_\pi = 2.47 \cdot 10^4$ MeV$^{1.7}$/(g · s · sr) was selected to minimize overall difference between experimental data and calculated spectrum. Fig. 3 shows a good agreement between calculation results and experimental data.

In Fig. 4, the ratio of experimental data to the calculated spectrum is shown. From this figure one can see that calculated spectrum describes well all experiments, disagreement for most part of points is in the range about 20% and does not exceed the difference between different experimental results. In Fig. 5, comparison of calculation results with experimental data for zenith angles 75° (Kiel-DESY [43]), 85° and 88.5° (DEIS [44], MUTRON [45]) is shown. Comparison also shows a good agreement between calculations and experimental data for near-horizontal directions. In Fig. 6, the ratio of these experimental data to calculated spectra is shown. Disagreement for most part of points is within about 15%.

So one can draw a conclusion that in a wide range of zenith angles and momentums a good agreement between muon spectrum calculations and experimental data is observed. Hence we can use the equations for muon spectrum calculations in order to obtain DTC.

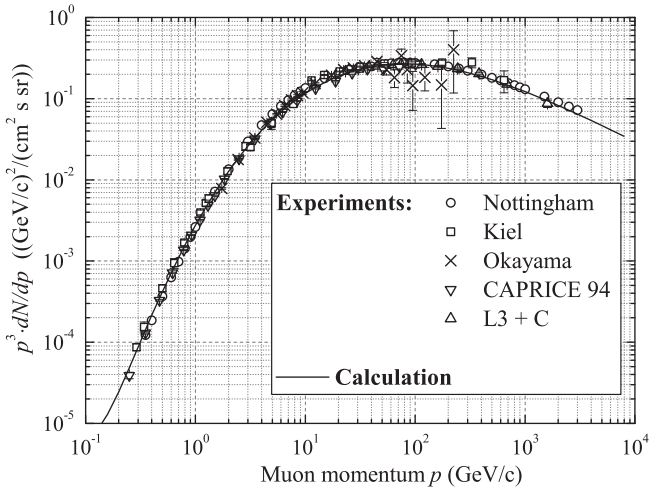

Fig. 3. Comparison of calculated muon spectrum with experimental data for vertical direction (Nottingham, Rastin fit [39], Kiel [40], Okayama [18], CAPRICE 94 [41], L3+C [42]).

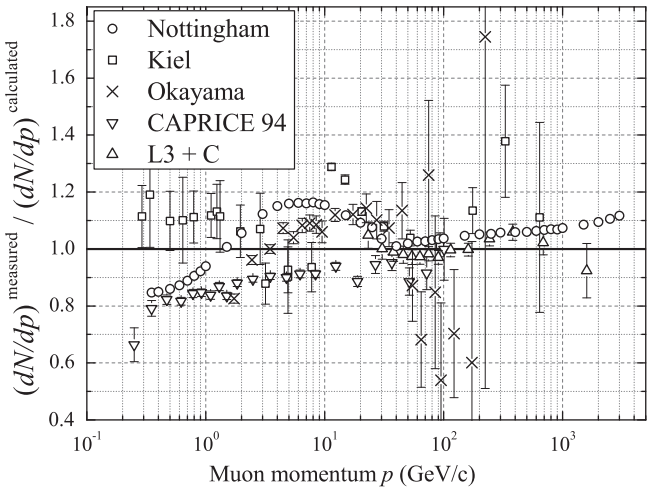

Fig. 4. The ratio of experimental data (Nottingham, Rastin fit [39], Kiel [40], Okayama [18], CAPRICE 94 [41], L3+C [42]) to calculated spectrum for zenith angle $\theta = 0°$.

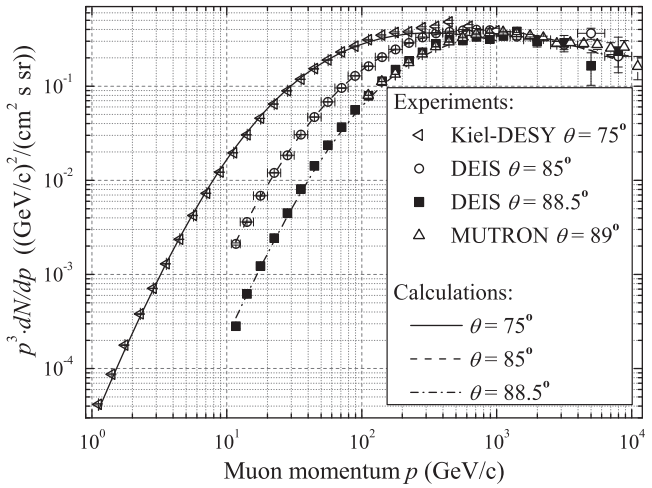

Fig. 5. Comparison of calculated muon spectra for near-horizontal directions with experimental data (Kiel-DESY [43], DEIS [44] and MUTRON [45]).

5. Calculation of differential temperature coefficients

If atmospheric temperature is changed by $\Delta T(h)$ (h is the atmospheric depth in atm) the standard muon flux $N_0(E_{min},X,\theta)$ at observation level X will be changed by $\Delta N_T(E_{min},X,\theta)$ and the relative change of the muon flux can be written in a following way [5]:

$$\Delta N_T(E_{min},X,\theta)/N_0(E_{min},X,\theta)\cdot 100\% = \int_0^X W_T(E_{min},X,h,\theta)\Delta T(h)dh \approx \sum_i W_T(E_{min},X,h_i,\theta)\Delta T(h_i)\Delta h_i, \quad (13)$$

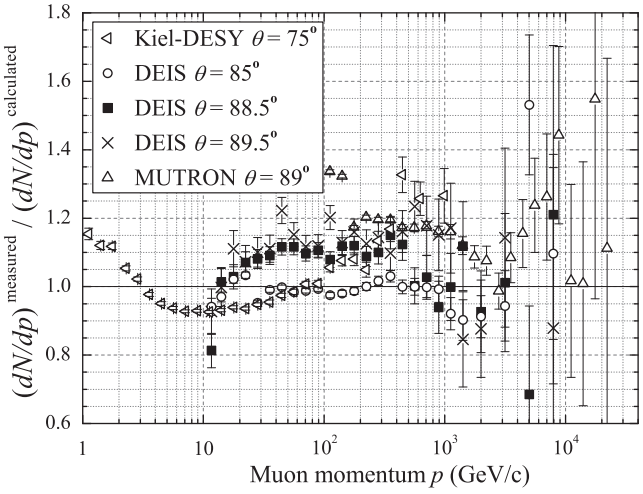

Fig. 6. The ratio of experimental data (Kiel-DESY [43], DEIS [44] and MUTRON [45]) to calculated spectrum for near-horizontal directions.

here the function $W_T(E_{min},X,h,\theta)$ is called DTC. Hereafter, the value of vertical step Δh equals to 0.05 atm.

As we have already mentioned, DTC can be found on the basis of the formulas describing muon production and propagation in the atmosphere. To obtain the expression for $\Delta N(E_{min},X,\theta)$, it is necessary to vary the function $N(E_{min},X,\theta)$ with respect to temperature at constant atmospheric pressure P:

$$\Delta N(E_{min},X,\theta)=\sum_\eta\int_{E_{min}}^{\infty}dE\int_0^{z_X}dz\int_0^{z}dz'\times\int_\varepsilon^{(m_\eta/m_\mu)^2\varepsilon}dE_\eta F_\eta(E,X,\theta,z,z',E_\eta)\cdot\left(\frac{\delta T(z)}{T(z)}-\frac{m_\eta c^2R}{c\tau_\eta E_\eta M}\int_{z'}^{z}\frac{\delta T(y)dy}{P(y)}-\frac{m_\mu c^2R}{c\tau_\mu M}\int_z^{z_X}\frac{\delta T(y)dy}{\varepsilon(E,z_X-y)P(y)}\right). \quad (14)$$

The factor in parentheses is in agreement (up to dimensions of quantities) with formula given by Dorman and Yanke (see [5]) while the function $F_\eta(E,X,\theta,z,z',E_\eta)$ being used in [5] contains many simplifications and approximations (see below). First two terms in parentheses in the integral reflect the change of muon flux because of the change of pion and kaon decay probability; the third term reflects the variation of muon flux because of changes of muon decay probability. Thus, the temperature effect can be divided in two components (so-called meson and muon effects):

$$W_T(E_{min},X,h,\theta)=W_T^\eta(E_{min},X,h,\theta)+W_T^\mu(E_{min},X,h,\theta). \quad (15)$$

To obtain $W_T(E_{min},X,h,\theta)$ it is necessary to combine Eqs. (13) and (14), then to take $\Delta T(h)$ equals to Dirac function $\delta(h)$. After transformation we obtain formulas for DTC calculation:

$$W_T^\eta(E_{min},X,h,\theta)=\frac{100\%}{N_0(E_{min},X,\theta)}\cdot\sum_\eta\left[\frac{1}{T(z_h)}\int_{E_{min}}^{\infty}dE\int_0^{z_h}dz'\times\int_\varepsilon^{(m_\eta^2/m_\mu^2)\varepsilon}dE_\eta F_\eta(E,X,\theta,z_h,z',E_\eta)+\int_{E_{min}}^{\infty}dE\int_{z_h}^{z_X}dz\int_0^{z_h}dz'\int_\varepsilon^{(m_\eta^2/m_\mu^2)\varepsilon}dE_\eta\times F(E,X,\theta,z,z',E_\eta)\cdot\left(\frac{-m_\eta c^2R}{c\tau_\eta E_\eta MP(z_h)}\right)\right], \quad (16)$$

$$W_T^\mu(E_{min},X,h,\theta)=\frac{100\%}{N_0(E_{min},X,\theta)}\cdot\sum_\eta\int_{E_{min}}^{\infty}dE\int_0^{z_h}dz\int_0^{z}dz'\times\int_\varepsilon^{(m_\eta^2/m_\mu^2)\varepsilon}dE_\eta F_\eta(E,X,\theta,z,z',E_\eta)\cdot\left(\frac{-m_\mu c^2R}{c\tau_\mu M\varepsilon(E,z_X-z_h)P(z_h)}\right). \quad (17)$$

The paths z_h, z_X along the trajectory of the particle (in g/cm^2) correspond to the depths h and X (see Fig. 1).

The sign of the meson effect W_T^η is positive, since if the temperature increases, the atmosphere expands, density of air decreases and the probability of the interaction of mesons (kaons and pions) at unit of geometric path becomes smaller, hence decay probability becomes higher. Sign of the muon effect W_T^μ is negative, because if the temperature increases and the atmosphere expands, the geometric path from generation level to registration point becomes longer, so higher number of muons will decay. The relation between absolute values of these effects depends on E_{min}. In case of low threshold energies the absolute value of the muon effect W_T^μ is greater than the value of meson effect W_T^η, and the sign of the total effect W_T is negative. In case of high threshold energies, the muon effect degrades (muons have not enough time to decay in the atmosphere) and the sign of the total effect becomes positive.

DTCs were calculated for six values of zenith angle (0°, 15°, 30°, 45°, 60° and 75°) and for two types of detectors: muon telescopes (threshold energy does not depend on zenith angle, E_{min} = const) and muon hodoscopes (threshold energy depends on zenith angle as E_{min} = const/cosθ). DTCs were calculated for four values of this constant: 0.4, 0.75, 1 and 1.25 GeV; calculation results are presented in Tables 2–9 in Appendix A.

Results of W_T^μ and W_T^η calculations for E_{min} = 0.4 GeV and six values of zenith angle are shown in Fig. 7. As it is seen, W_T^μ is negative, W_T^η is positive and the absolute value of the muon effect W_T^μ is greater than the value of meson effect W_T^η. At h > 0.7 atm contribution of meson effect to the total effect is negligible because of small amount of mesons at these depths.

The value of constant in threshold energy (0.4 GeV) is close to the threshold energy of existing muon hodoscopes [30]. So in following sections we will consider corrections for temperature effect for this energy. Total effect W_T for E_{min} = 0.4 GeV is presented in Fig. 8. For the comparison, total effect W_T for E_{min} = 0.4 GeV/cosθ is presented in Fig. 9.

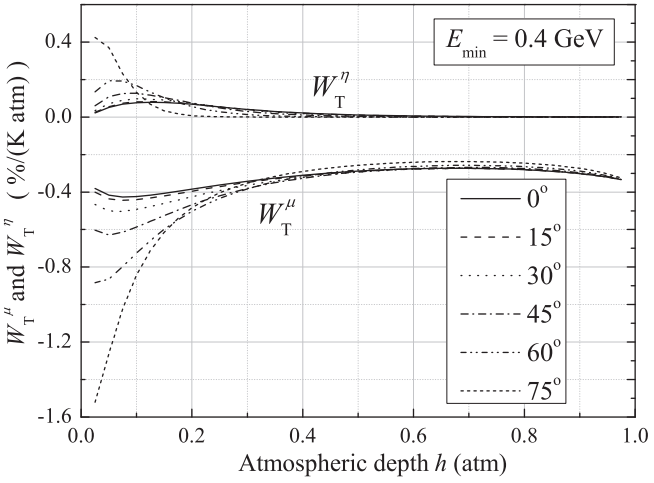

Fig. 7. Muon W_T^μ and meson W_T^η differential temperature coefficients calculated for E_{min} = 0.4 GeV and several zenith angles.

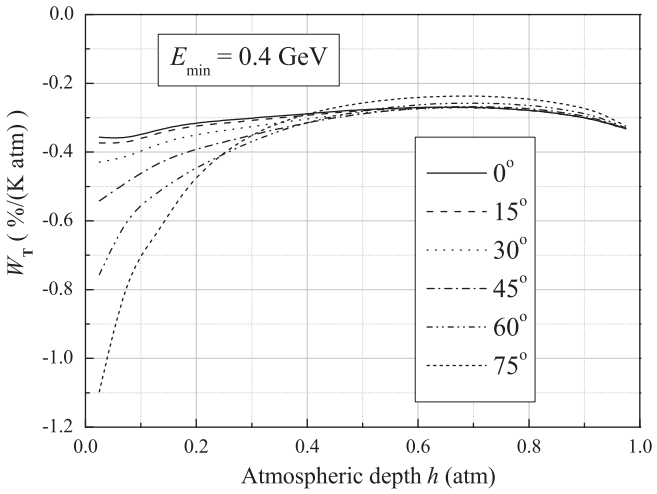

Fig. 8. Total differential temperature coefficients W_T calculated for E_{min} = 0.4 GeV and several zenith angles.

Examples of dependences of DTCs on atmospheric depth h for $\theta = 0°$ and five values of threshold energy (0.4, 1, 4.5, 10, and 43 GeV) are shown in Fig. 10. From this figure one can see that for threshold energies above 10 GeV DTC becomes positive in a significant part of atmosphere thickness.

6. Comparison with results of earlier calculations

Differential temperature coefficients calculated by Dorman and Yanke [5] for E_{min} = 0.4 GeV and four values of zenith angle are shown in Fig. 11. DTCs for large zenith angles are in a good qualitative agreement with our results (Fig. 8). But for zenith angle $\theta = 0°$, the dependence of $W_T(h)$ seriously differs. One should note however that a direct comparison of DTCs obtained in two works is not quite justified because in calculations [5] somewhat differing parameters were used (γ = 2.5, L_p = 120 g/cm^2, λ_π = 60 g/cm^2), contribution of kaons to muon flux was not taken into account, muon energy loss was considered as constant (2 MeV $\cdot$ g^{-1} $\cdot$ cm^2), and a simplified model of atmosphere was used.

To understand the source of disagreement in the dependence of $W_T(h)$, additional calculations were carried out. Approximations

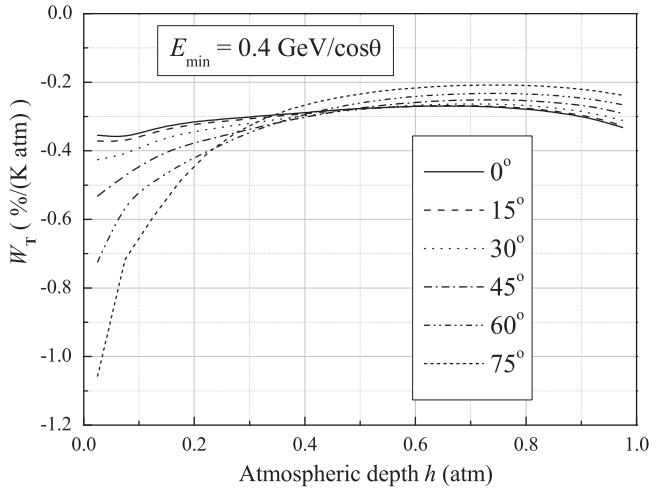

Fig. 9. Total differential temperature coefficients W_T calculated for E_{min} = 0.4 GeV/cosθ and several zenith angles.

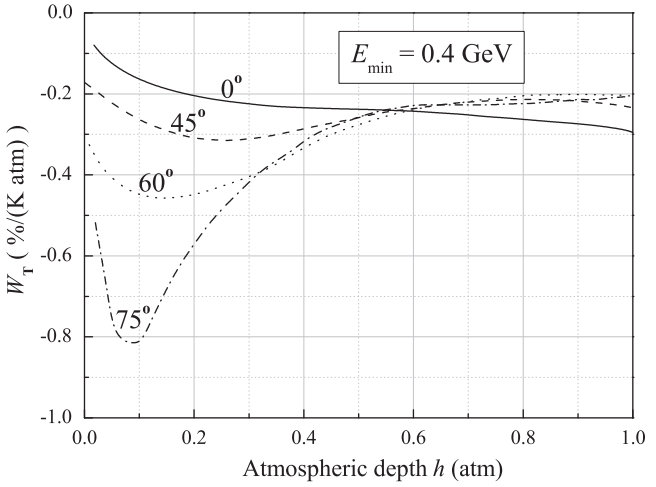

Fig. 11. Total differential temperature coefficients W_T for several values of zenith angle calculated in [5].

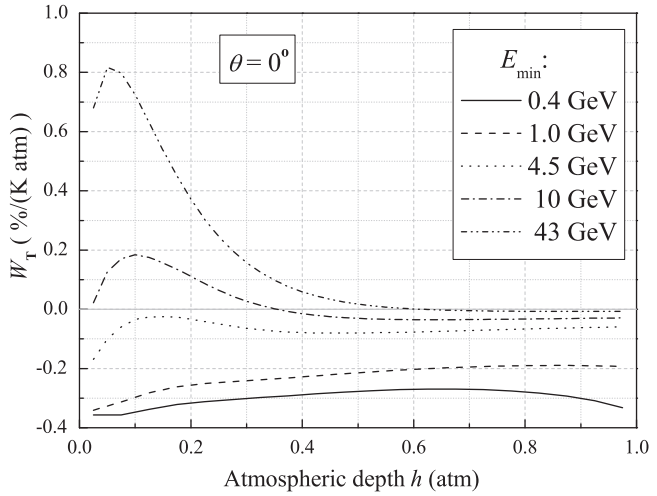

Fig. 10. Total differential temperature coefficients W_T calculated for $\theta = 0°$ and several values of threshold energy.

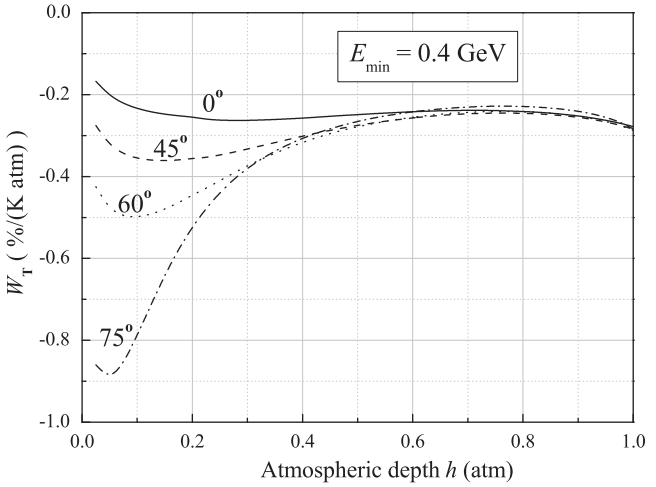

Fig. 12. Total differential temperature coefficients W_T for several values of zenith angle calculated in our work with approximations used in [5].

and values of parameters used in [5] were introduced in our model of DTC calculations, contribution of kaons was switched off. Results of additional calculations are presented in Fig. 12. Comparison of DTC in Figs. 8, 11 and 12 shows that disagreement in dependence $W_T(h)$ for vertical direction cannot be explained by physical approximations used in [5]. Differences between calculation results, probably, can be related with insufficient precision of numerical calculations in [5].

In the work of Maeda [32], an empirical formula for muon production spectrum was used: $P^{\eta\mu}(p,z) = A/(a' + r(p))^{3.38}\exp(-z/L_n)$, here z is the depth of muon generation along the track (in g/cm^2), r is the residual range in air (in g/cm^2) of muons with momentum p, A and a' are constants, $L_n = 120$ g/cm^2 is attenuation length of primary nucleons. In DTC calculations, two-layer stationary spherical model of atmosphere was used, dependences of meson and muon decay probability on atmospheric temperature, and of the energy loss on muon energy were taken into account. Pion interaction mean free path was taken as $\lambda_\pi = 60$ g/cm^2, contribution of kaons to muon flux was not taken into account. In this work DTCs were calculated for zenith angles 0°, 60°, 75° and 86° and six values of threshold energy (0.5, 2.2, 4.5, 10, 21 and 43 GeV). DTCs calculated in [32] for $\theta = 0°$ are presented in Fig. 13. In order to compare our results with results of [32], calculations of DTC by formulas (16) and (17) for these threshold energies were carried out (Fig. 14). As it is seen, the comparison of calculation results of our work with calculations [32] shows a qualitative agreement, however quantitatively the results differ by tens percent. Difference, probably, can be caused by approximations used in [32].

The best agreement is found between the results of our calculations and the calculations of Sagisaka [33]. In this work US standard atmosphere model was used. Contributions of both pions and kaons and also of primary protons and heavier nuclei were taken into account. The following values of interaction mean free paths were used: $\lambda_N = 80$ g/cm^2, $\lambda_\pi = 120$ g/cm^2, $\lambda_K = 140$ g/cm^2. For the meson generation function, numerical solution of cascade equations based on parameterisations of the available accelerator data on hadron interactions was utilised [46]. Dependence of muon energy loss on muon energy was neglected. DTCs were calculated for zenith angles 0°, 32°, 48° and 64°, four observational atmospheric depths (550, 740, 920 and 1030 g/cm^2) and eight values of threshold energy (0.32, 1.0, 3.2, 10, 32, 100, 320 and 1000 GeV). Differential temperature coefficients calculated by Sagisaka [33] for vertical direction, for sea level and various values

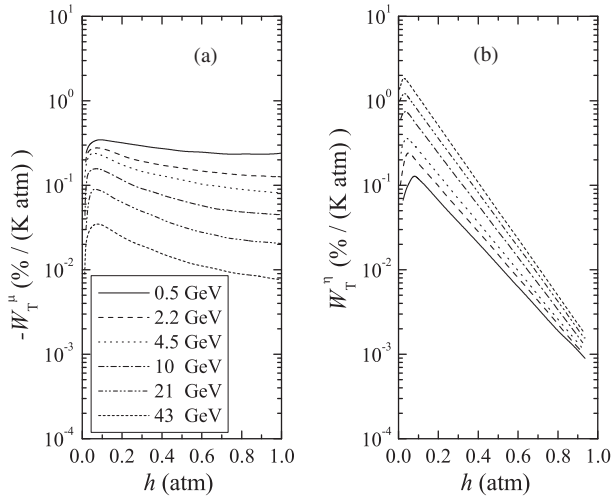

Fig. 13. Muon W_T^{μ} (a) and meson W_T^{η} (b) differential temperature coefficients calculated in [32] for $\theta = 0°$ and for several values of threshold energy.

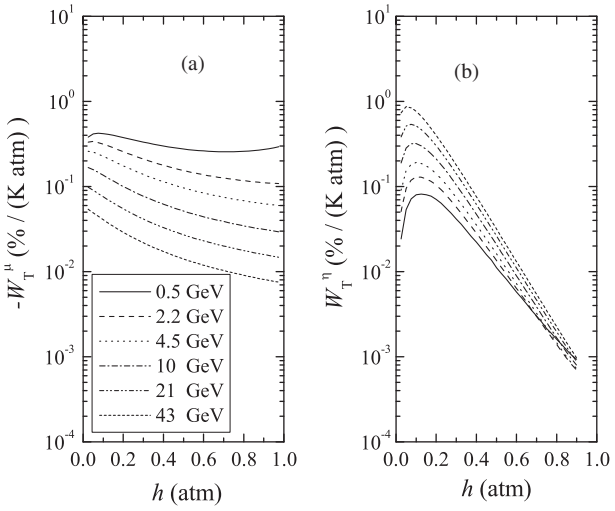

Fig. 14. Muon W_T^{μ} (a) and meson W_T^{η} (b) differential temperature coefficients calculated in present work for the same values of threshold energy as in [32].

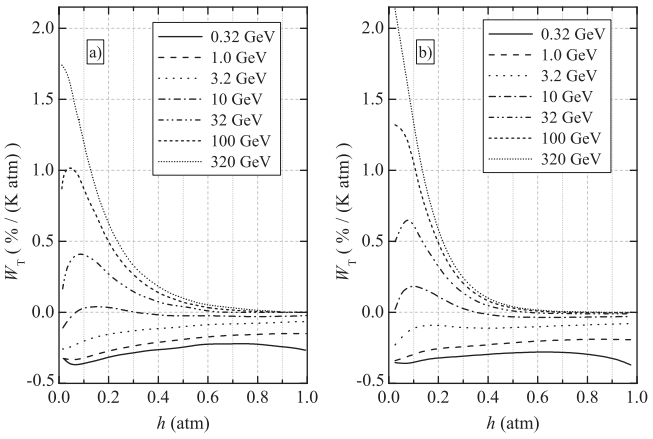

Fig. 15. Differential temperature coefficients W_T for vertical direction: (a) calculated in [33]; (b) calculated in present work for the same values of threshold energy as in [33].

of threshold energies are shown in Fig. 15a. These DTCs are in good agreement with our results (see Fig. 15b) except of the region of intermediate threshold energies (3–100 GeV) at small atmospheric depths ($h < 0.1$ atm).

7. The use of DTC

For estimation of the precision of corrections for temperature effect, integral muon intensity was calculated directly by formulae (8) for three types of atmospheric temperature profile (AS, A1 and A2, see the description of atmospheric models above). Relative difference between calculated integral muon intensity $N(E_{min},X,\theta)$ and value $N_0(E_{min},X,\theta)$ for standard atmosphere $(N - N_0)/N_0 \cdot 100\%$ is shown in Fig. 16 by full symbols (for higher temperature the intensity is lower, and vice versa). One can see that it only slightly depends on zenith angle. Difference between maximum and minimum values of muon intensity for different versions of atmosphere reaches about 8%. After correction of muon counting rate for temperature effect using formula (13) (open symbols in Fig. 16) the difference of results $(N^{corr} - N_0)/N_0 \cdot 100\%$ for various atmosphere models does not exceed 0.3%. The non-zero value of this difference is explained by uncertainties which are caused by

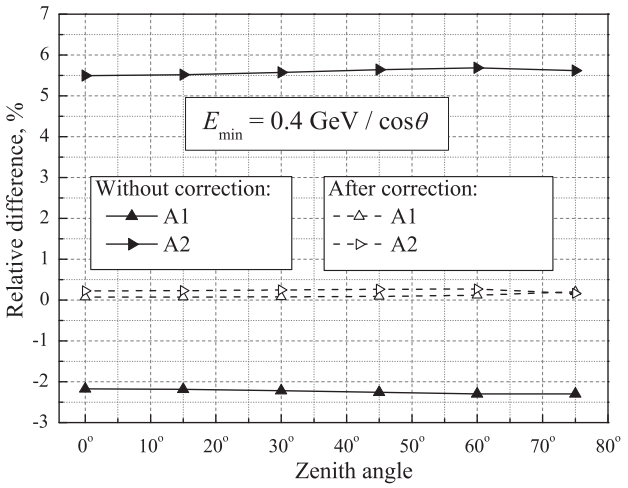

Fig. 16. Relative difference between calculated integral muon intensity for different atmospheric conditions and standard value. Differences without correction for temperature effect are shown by full symbols, after correction by open symbols. A1 and A2 are different atmospheric temperature profiles.

the use of summation instead of exact integral (see formulae (13)). Calculations show that for telescopes with E_{min} = 0.4 GeV the precision of corrections is similar.

Obtained DTC were applied for correction of the data of URAGAN [30], wide-aperture precision muon hodoscope which is used to study atmospheric and heliospheric processes responsible for variations in the muon flux at the Earth surface.

The hodoscope consists of separate horizontal assemblies (supermodules) with the area of 11.5 m^2 each. Three supermodules of hodoscope are now under operation in the exposure mode. Each supermodule consists of eight layers of streamer tube chambers equipped with a two-coordinate system of external readout strips. In every layer, there are 320 *X* channels and 288 *Y* channels with pitches of 1.0 and 1.2 cm, respectively. The layers are interleaved with 5 cm thick foam–plastic sheets. A limited streamer mode is maintained in the chambers by means of the three-component gas mixture (argon + CO_2 + *n*-pentane) and proper selection of the operating voltage. The supermodule detects muons with a high spatial and angular accuracies (1 cm and 1°, respectively) over a wide range of zenith angles (0–80°).

Examples of 1 h average intensity of reconstructed events for two zenith angle intervals ($10° < \theta < 20°$ and $40° < \theta < 50°$) in one supermodule of the URAGAN hodoscope over the period March 2007–December 2008 without corrections for atmospheric effects are presented in Fig. 17a and b by light grey lines. Data are shown for two points daily (00:00 and 12:00 UT) when the information about temperature profile of the atmosphere from balloon flights was available [38]. Difference between maximum and minimum intensity reaches about 15%. Using the pressure values and the

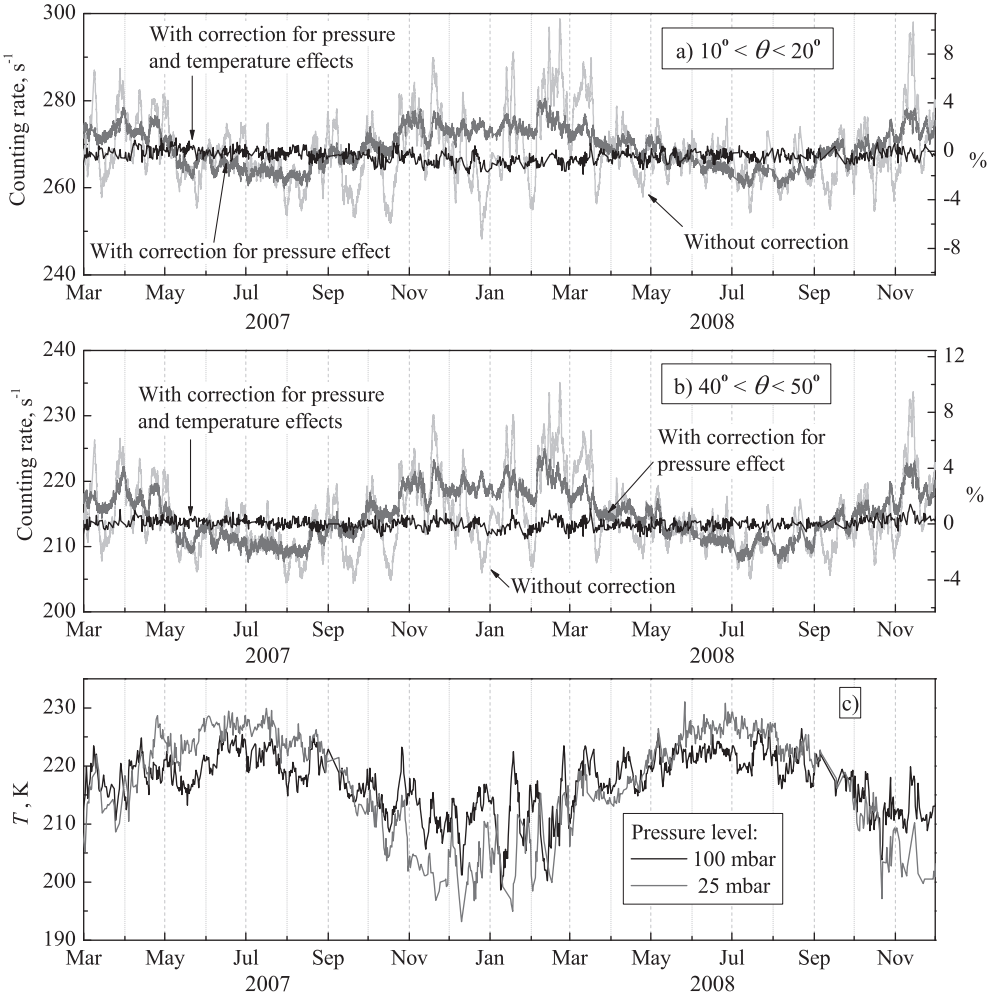

Fig. 17. One hour average counting rate of reconstructed events in the URAGAN supermodule during March 2007–December 2008: (a) counting rate for zenith angle interval $10° < \theta < 20°$; (b) counting rate for zenith angle interval $40° < \theta < 50°$ and (c) temperature of air at 100 and 25 mbar pressure levels (two balloon flights daily).

counting rates in the periods of calm geomagnetic situation, one can determine the barometric coefficient. The absolute value of barometric coefficient decreases with increase of zenith angle. For two angular bins presented in Fig. 17 the values of barometric coefficient were found equal to −0.22 and −0.16%/mbar, respectively. For the integral counting rate of URAGAN supermodule barometric coefficient is about −0.18%/mbar. Intensity of reconstructed events with corrections for pressure effect are presented in Fig. 17a and b by grey lines. A seasonal variation caused by temperature effect in cosmic-ray muon flux becomes well visible and it is about 8%. On the background of the seasonal trend, smaller variations of about 1–2% with duration of few days–few weaks are also observed. In the same figure (Fig. 17c) temperature of air at 100 and 25 mbar pressure levels is shown. Intensity of reconstructed events with corrections for both barometric and temperature effects are presented in Fig. 17a and b by black lines. March 2007–December 2008 was a period of quiet heliospheric weather and therefore there was no sharp changes in corrected muon counting rate. Thus, the use of the calculated DTC for temperature effect corrections for URAGAN data decreases the difference between the current and standard value of muon counting rate to several tenths of percent. For convenience, on the right axis of Fig. 17a and b relative difference between current and average corrected counting rate is shown (in %).

8. Conclusion

Differential muon spectra and differential temperature coefficients were calculated for presently known parameters of interactions of primary and secondary particles with air, for six-layer spherical model of atmosphere, taking into account contributions of both pions and kaons to muon flux. In a wide range of zenith angles and momenta a good agreement between muon spectrum calculations and experimental data of magnetic spectrometers is observed. Using obtained formulas for muon intensity as a non-disturbed level, analytic expressions for differential temperature coefficients have been derived. In Appendix A, calculated values of DTC for several threshold energies (0.4, 0.75, 1 and 1.25 GeV) and zenith angles (0°, 15°, 30°, 45°, 60° and 75°) and for two types of detectors: rotatable muon telescopes (threshold energy does not depend on zenith angle, E_{min} = const) and muon hodoscopes (threshold energy depends on zenith angle as E_{min} = const/cosθ) are presented.

The use of calculated DTC for temperature effect corrections decreases the difference between the current and standard values of integral muon intensity from several percent to several tenths of percent for any zenith angle.

Results of present DTC calculations are only in qualitative agreement with the preceding publications, whereas quantitative differences amount to tens percent. These differences can be caused by various approximations in earlier works.

Acknowledgements

The research has been performed in Scientific and Educational Centre NEVOD with the support of Ministry of Education and Science (Contract No. 02.518.11.7166), Russian Foundation for Basic Research (Grant 08-02-01204-a), the Federal Target Program "Scientific and educational cadres for innovative Russia" and the grant of the leading scientific school NSh-5712.2010.2.

Appendix A. Differential temperature coefficients

Total differential temperature coefficients ($W_T(E_{min},X,h,\theta)$, %/(K · atm)) are presented for four values of threshold energy

Table 2
Total differential temperature coefficients for E_{min} = 0.4 GeV and six values of zenith angle.

h, atm	θ = 0°	θ = 15°	θ = 30°	θ = 45°	θ = 60°	θ = 75°
0.025	−0.356	−0.373	−0.429	−0.542	−0.756	−1.140
0.075	−0.357	−0.370	−0.412	−0.487	−0.604	−0.780
0.125	−0.338	−0.349	−0.382	−0.439	−0.524	−0.639
0.175	−0.322	−0.331	−0.358	−0.405	−0.469	−0.522
0.225	−0.312	−0.320	−0.343	−0.381	−0.426	−0.435
0.275	−0.305	−0.312	−0.332	−0.361	−0.387	−0.374
0.325	−0.298	−0.304	−0.320	−0.341	−0.354	−0.332
0.375	−0.292	−0.297	−0.309	−0.323	−0.326	−0.301
0.425	−0.285	−0.289	−0.299	−0.308	−0.305	−0.279
0.475	−0.279	−0.282	−0.289	−0.294	−0.288	−0.263
0.525	−0.275	−0.277	−0.282	−0.284	−0.275	−0.252
0.575	−0.271	−0.273	−0.276	−0.276	−0.266	−0.244
0.625	−0.270	−0.271	−0.273	−0.271	−0.260	−0.239
0.675	−0.269	−0.270	−0.271	−0.268	−0.258	−0.237
0.725	−0.271	−0.272	−0.272	−0.269	−0.258	−0.238
0.775	−0.275	−0.276	−0.275	−0.272	−0.261	−0.242
0.825	−0.283	−0.283	−0.282	−0.278	−0.268	−0.250
0.875	−0.293	−0.293	−0.293	−0.289	−0.280	−0.264
0.925	−0.309	−0.309	−0.308	−0.305	−0.299	−0.286
0.975	−0.332	−0.332	−0.332	−0.332	−0.330	−0.325

Table 3
Total differential temperature coefficients for E_{min} = 0.75 GeV and six values of zenith angle.

h, atm	θ = 0°	θ = 15°	θ = 30°	θ = 45°	θ = 60°	θ = 75°
0.025	−0.350	−0.365	−0.417	−0.523	−0.728	−1.120
0.075	−0.334	−0.346	−0.384	−0.455	−0.573	−0.764
0.125	−0.307	−0.317	−0.348	−0.405	−0.496	−0.628
0.175	−0.288	−0.296	−0.323	−0.372	−0.445	−0.513
0.225	−0.277	−0.285	−0.309	−0.350	−0.404	−0.427
0.275	−0.270	−0.277	−0.297	−0.331	−0.367	−0.367
0.325	−0.263	−0.269	−0.286	−0.312	−0.335	−0.325
0.375	−0.256	−0.261	−0.275	−0.295	−0.309	−0.295
0.425	−0.248	−0.253	−0.264	−0.280	−0.287	−0.273
0.475	−0.241	−0.245	−0.255	−0.266	−0.270	−0.257
0.525	−0.235	−0.238	−0.246	−0.255	−0.258	−0.246
0.575	−0.230	−0.233	−0.239	−0.247	−0.248	−0.237
0.625	−0.226	−0.228	−0.234	−0.240	−0.241	−0.232
0.675	−0.222	−0.224	−0.230	−0.236	−0.237	−0.229
0.725	−0.220	−0.222	−0.227	−0.233	−0.236	−0.230
0.775	−0.220	−0.222	−0.227	−0.233	−0.236	−0.232
0.825	−0.220	−0.222	−0.228	−0.234	−0.240	−0.239
0.875	−0.223	−0.225	−0.230	−0.238	−0.246	−0.249
0.925	−0.227	−0.229	−0.235	−0.245	−0.256	−0.265
0.975	−0.232	−0.235	−0.243	−0.255	−0.272	−0.292

Table 4
Total differential temperature coefficients for E_{min} = 1 GeV and six values of zenith angle.

h, atm	θ = 0°	θ = 15°	θ = 30°	θ = 45°	θ = 60°	θ = 75°
0.025	−0.341	−0.356	−0.405	−0.508	−0.709	−1.100
0.075	−0.313	−0.324	−0.360	−0.430	−0.549	−0.750
0.125	−0.282	−0.291	−0.322	−0.379	−0.475	−0.618
0.175	−0.262	−0.270	−0.297	−0.347	−0.427	−0.505
0.225	−0.251	−0.259	−0.283	−0.327	−0.388	−0.421
0.275	−0.245	−0.252	−0.273	−0.310	−0.352	−0.362
0.325	−0.238	−0.244	−0.263	−0.292	−0.321	−0.320
0.375	−0.232	−0.237	−0.253	−0.276	−0.295	−0.290
0.425	−0.224	−0.229	−0.242	−0.261	−0.274	−0.268
0.475	−0.217	−0.221	−0.233	−0.248	−0.258	−0.252
0.525	−0.211	−0.215	−0.224	−0.237	−0.245	−0.240
0.575	−0.205	−0.208	−0.217	−0.228	−0.235	−0.232
0.625	−0.200	−0.203	−0.211	−0.221	−0.228	−0.226
0.675	−0.196	−0.199	−0.206	−0.215	−0.223	−0.223
0.725	−0.193	−0.196	−0.202	−0.212	−0.220	−0.223
0.775	−0.191	−0.193	−0.200	−0.210	−0.220	−0.225
0.825	−0.190	−0.192	−0.199	−0.210	−0.222	−0.230
0.875	−0.190	−0.192	−0.199	−0.211	−0.225	−0.238
0.925	−0.191	−0.193	−0.201	−0.214	−0.232	−0.251
0.975	−0.192	−0.195	−0.205	−0.220	−0.242	−0.272

Table 5
Total differential temperature coefficients for E_{min} = 1.25 GeV and six values of zenith angle.

h, atm	$\theta = 0°$	$\theta = 15°$	$\theta = 30°$	$\theta = 45°$	$\theta = 60°$	$\theta = 75°$
0.025	−0.330	−0.344	−0.392	−0.492	−0.689	−1.080
0.075	−0.290	−0.301	−0.336	−0.405	−0.524	−0.735
0.125	−0.257	−0.266	−0.296	−0.353	−0.453	−0.608
0.175	−0.236	−0.245	−0.272	−0.323	−0.408	−0.497
0.225	−0.227	−0.235	−0.260	−0.305	−0.371	−0.414
0.275	−0.222	−0.229	−0.251	−0.290	−0.338	−0.355
0.325	−0.216	−0.222	−0.242	−0.274	−0.308	−0.314
0.375	−0.210	−0.216	−0.233	−0.258	−0.283	−0.285
0.425	−0.204	−0.208	−0.223	−0.243	−0.262	−0.263
0.475	−0.197	−0.201	−0.213	−0.231	−0.246	−0.247
0.525	−0.191	−0.195	−0.205	−0.220	−0.233	−0.235
0.575	−0.185	−0.188	−0.198	−0.211	−0.223	−0.226
0.625	−0.180	−0.183	−0.191	−0.204	−0.215	−0.220
0.675	−0.175	−0.178	−0.186	−0.198	−0.210	−0.217
0.725	−0.172	−0.174	−0.182	−0.194	−0.207	−0.216
0.775	−0.169	−0.171	−0.179	−0.191	−0.205	−0.217
0.825	−0.167	−0.169	−0.177	−0.189	−0.205	−0.221
0.875	−0.165	−0.168	−0.176	−0.189	−0.208	−0.228
0.925	−0.165	−0.168	−0.176	−0.191	−0.212	−0.239
0.975	−0.165	−0.168	−0.177	−0.194	−0.218	−0.255

Table 6
Total differential temperature coefficients for E_{min} = 0.4 GeV/cosθ and six values of zenith angle.

h, atm	$\theta = 0°$	$\theta = 15°$	$\theta = 30°$	$\theta = 45°$	$\theta = 60°$	$\theta = 75°$
0.025	−0.356	−0.372	−0.426	−0.532	−0.724	−1.060
0.075	−0.357	−0.369	−0.407	−0.473	−0.568	−0.717
0.125	−0.338	−0.348	−0.376	−0.424	−0.492	−0.595
0.175	−0.322	−0.329	−0.353	−0.390	−0.442	−0.487
0.225	−0.312	−0.318	−0.338	−0.367	−0.401	−0.405
0.275	−0.305	−0.311	−0.326	−0.347	−0.364	−0.348
0.325	−0.298	−0.303	−0.314	−0.328	−0.332	−0.307
0.375	−0.292	−0.295	−0.303	−0.310	−0.306	−0.278
0.425	−0.285	−0.288	−0.293	−0.294	−0.285	−0.256
0.475	−0.279	−0.281	−0.283	−0.281	−0.268	−0.240
0.525	−0.275	−0.276	−0.276	−0.270	−0.255	−0.229
0.575	−0.271	−0.271	−0.270	−0.262	−0.245	−0.220
0.625	−0.270	−0.269	−0.266	−0.256	−0.239	−0.214
0.675	−0.269	−0.268	−0.264	−0.253	−0.234	−0.210
0.725	−0.271	−0.270	−0.264	−0.251	−0.233	−0.208
0.775	−0.275	−0.273	−0.266	−0.252	−0.233	−0.208
0.825	−0.283	−0.280	−0.271	−0.256	−0.236	−0.211
0.875	−0.293	−0.290	−0.280	−0.263	−0.242	−0.216
0.925	−0.309	−0.305	−0.293	−0.274	−0.251	−0.225
0.975	−0.332	−0.327	−0.312	−0.290	−0.265	−0.238

Table 7
Total differential temperature coefficients for E_{min} = 0.75 GeV/cosθ and six values of zenith angle.

h, atm	$\theta = 0°$	$\theta = 15°$	$\theta = 30°$	$\theta = 45°$	$\theta = 60°$	$\theta = 75°$
0.025	−0.350	−0.365	−0.412	−0.504	−0.668	−0.93
0.075	−0.334	−0.343	−0.373	−0.424	−0.499	−0.631
0.125	−0.307	−0.314	−0.336	−0.372	−0.431	−0.536
0.175	−0.288	−0.294	−0.311	−0.341	−0.390	−0.442
0.225	−0.277	−0.282	−0.297	−0.322	−0.356	−0.368
0.275	−0.270	−0.274	−0.286	−0.305	−0.324	−0.314
0.325	−0.263	−0.266	−0.275	−0.288	−0.295	−0.277
0.375	−0.256	−0.258	−0.265	−0.271	−0.270	−0.249
0.425	−0.248	−0.250	−0.254	−0.256	−0.250	−0.229
0.475	−0.241	−0.242	−0.244	−0.243	−0.234	−0.213
0.525	−0.235	−0.236	−0.236	−0.232	−0.222	−0.201
0.575	−0.230	−0.230	−0.228	−0.223	−0.212	−0.192
0.625	−0.226	−0.225	−0.223	−0.216	−0.204	−0.185
0.675	−0.222	−0.222	−0.218	−0.211	−0.198	−0.181
0.725	−0.220	−0.219	−0.215	−0.207	−0.194	−0.177
0.775	−0.220	−0.218	−0.213	−0.205	−0.192	−0.175
0.825	−0.220	−0.219	−0.213	−0.204	−0.191	−0.175
0.875	−0.223	−0.221	−0.215	−0.205	−0.192	−0.176
0.925	−0.227	−0.224	−0.218	−0.208	−0.195	−0.178
0.975	−0.232	−0.230	−0.223	−0.213	−0.199	−0.183

Table 8
Total differential temperature coefficients for E_{min} = 1 GeV/cosθ and six values of zenith angle.

h, atm	$\theta = 0°$	$\theta = 15°$	$\theta = 30°$	$\theta = 45°$	$\theta = 60°$	$\theta = 75°$
0.025	−0.341	−0.354	−0.397	−0.480	−0.626	−0.839
0.075	−0.313	−0.321	−0.345	−0.388	−0.450	−0.573
0.125	−0.282	−0.288	−0.305	−0.336	−0.390	−0.498
0.175	−0.262	−0.266	−0.281	−0.308	−0.356	−0.413
0.225	−0.251	−0.255	−0.268	−0.292	−0.327	−0.343
0.275	−0.245	−0.248	−0.259	−0.277	−0.298	−0.293
0.325	−0.238	−0.241	−0.250	−0.262	−0.272	−0.257
0.375	−0.232	−0.234	−0.240	−0.247	−0.249	−0.231
0.425	−0.224	−0.226	−0.230	−0.233	−0.230	−0.212
0.475	−0.217	−0.218	−0.220	−0.221	−0.214	−0.197
0.525	−0.211	−0.212	−0.212	−0.210	−0.202	−0.185
0.575	−0.205	−0.205	−0.205	−0.201	−0.192	−0.176
0.625	−0.200	−0.200	−0.198	−0.194	−0.184	−0.169
0.675	−0.196	−0.196	−0.193	−0.188	−0.178	−0.164
0.725	−0.193	−0.192	−0.189	−0.183	−0.174	−0.160
0.775	−0.191	−0.190	−0.186	−0.180	−0.170	−0.157
0.825	−0.190	−0.189	−0.185	−0.178	−0.168	−0.156
0.875	−0.190	−0.188	−0.184	−0.177	−0.168	−0.155
0.925	−0.191	−0.189	−0.185	−0.178	−0.168	−0.156
0.975	−0.192	−0.191	−0.187	−0.179	−0.170	−0.158

Table 9
Total differential temperature coefficients for E_{min} = 1.25 GeV/cosθ and six values of zenith angle.

h, atm	$\theta = 0°$	$\theta = 15°$	$\theta = 30°$	$\theta = 45°$	$\theta = 60°$	$\theta = 75°$
0.025	−0.330	−0.342	−0.381	−0.456	−0.584	−0.751
0.075	−0.290	−0.297	−0.318	−0.353	−0.404	−0.519
0.125	−0.257	−0.262	−0.276	−0.302	−0.352	−0.463
0.175	−0.236	−0.241	−0.253	−0.278	−0.325	−0.387
0.225	−0.227	−0.231	−0.243	−0.265	−0.301	−0.322
0.275	−0.222	−0.225	−0.235	−0.253	−0.276	−0.275
0.325	−0.216	−0.219	−0.227	−0.240	−0.251	−0.240
0.375	−0.210	−0.213	−0.219	−0.227	−0.230	−0.216
0.425	−0.204	−0.205	−0.209	−0.214	−0.212	−0.197
0.475	−0.197	−0.198	−0.200	−0.202	−0.197	−0.182
0.525	−0.191	−0.191	−0.192	−0.191	−0.185	−0.171
0.575	−0.185	−0.185	−0.185	−0.183	−0.175	−0.162
0.625	−0.180	−0.180	−0.179	−0.175	−0.168	−0.155
0.675	−0.175	−0.175	−0.173	−0.169	−0.162	−0.150
0.725	−0.172	−0.171	−0.169	−0.164	−0.157	−0.145
0.775	−0.169	−0.168	−0.166	−0.161	−0.153	−0.142
0.825	−0.167	−0.166	−0.163	−0.158	−0.150	−0.140
0.875	−0.165	−0.164	−0.161	−0.156	−0.149	−0.139
0.925	−0.165	−0.164	−0.161	−0.155	−0.148	−0.138
0.975	−0.165	−0.164	−0.161	−0.156	−0.148	−0.139

E_{min} = const (muon telescopes) and for four values of E_{min} = const/cosθ (muon hodoscopes), and six values of zenith angle. Registration level X corresponds to sea level; h is the atmospheric vertical depth in atm (1 atm = 1033.23 g/cm^2).

References

[1] S.E. Forbush, I. Lange, Cosmic Ray Results, Res. Dept. Terr. Mag., vol. XX, Carnegie Inst., Washington, D.C., 1957.
[2] L.I. Dorman, Cosmic Ray Variations, Gostekhteorizdat, Moscow, 1957 (in English: US Department of Defense, Ohio Air-Force Base, 1958).
[3] D. Venkatensan, Badruddin, Space Sci. Rev. 52 (1989) 121–194.
[4] L.I. Dorman, Cosmic Rays in the Earth's Atmosphere and Underground, Kluwer Academic Publisher, 2004.
[5] L.I. Dorman, Meteorological Effects in Cosmic Rays, Nauka, Moscow, 1972 (in Russian).
[6] M.L. Duldig, Space Sci. Rev. 93 (2000) 207–226.
[7] L.I. Miroshnichenko, in: V.A. Matveev, V.A. Rubakov, Kh.S. Nirov (Eds.), Proceedings of the XII International School Particles and Cosmology, Institute of Nuclear Research of RAS, Moscow, 2004, pp. 96–100.
[8] A.H. Compton, E. Wollan, R.D. Bennet, Rev. Sci. Instrum. 5 (1934) 415–422.
[9] C. Morello, G. Novarra, Nucl. Instrum. Methods A 187 (1981) 533–538.
[10] Z.M. Karpova et al., Bull. RAS: Phys. 71 (7) (2007) 938–941.

[11] J.M. Ryan, in: Proceedings of the 26th ICRC, Salt Lake City, vol. 6, 1999, pp. 378–381.
[12] C. D'Andrea, J. Poirier, D.S. Balsara, Adv. Space Res. 44 (2009) 1247–1251.
[13] L.I. Dorman, Cosmic Rays: Variations and Space Explorations, North-Holland, Amsterdam, 1974.
[14] C. Grupen, B. Shwarts, Particle Detectors, University Press, Cambridge, 2008.
[15] B.G. Wilson, Can. J. Phys. 37 (1959) 19–29.
[16] N.L. Karmakar, A. Paul, N. Chaudhuri, Nuovo Cim. B 17 (1973) 173–186.
[17] D.P. Bhattacharyya, Phys. Rev. D 13 (1976) 566–570.
[18] Y. Yamashita et al., Nucl. Instrum. Methods A 374 (1996) 245–253.
[19] R. Wang, Astropart. Phys. 31 (2009) 149–155.
[20] M. Selvi, LVD Collaboration, in: Proceedings of the 31st ICRC (CD-disc), Section HE2.1, ID0766, 2009.
[21] J.K. de Jong, E.W. Grashorn, MINOS Collaboration, in: Proceedings of the 31st ICRC (CD-disc), Section HE2.1, ID1060, 2009.
[22] R.L. Chasson et al., in: Proceedings of the Ninth ICRC, London, vol. 1, 1965, pp. 282–284.
[23] Solar-Terrestrial Environment Laboratory, Nagoya University, Nagoya Multi-Directional Muon Telescope. Available from: <http://www.stelab.nagoya-u.ac.jp/ste-www1/div3/muon/dbtext22.pdf>.
[24] T. Kuwabara et al., Space Weather 4 (2006) S08001.
[25] V.V. Borog et al., in: Proceedings of the 24th ICRC, Roma, vol. 4, 1995, pp. 1291–1294.
[26] Y. Ohashi et al., in: Proceedings of the 25th ICRC, Durban, vol. 1, 1997, pp. 441–444.
[27] D.V. Chernov et al., in: Proceedings of the 29th ICRC, Pune, vol. 2, 2005, pp. 457–460.
[28] Y. Okazaki et al., ApJ 681 (2008) 693–707.
[29] D.A. Timashkov et al., in: Proceedings of the 30th ICRC, Merida, vol. 1, 2007, pp. 685–688.
[30] N.S. Barbashina et al., Instrum. Exp. Tech. 51 (2008) 180–186.
[31] A.G. Bogdanov et al., in: Proceedings of the 21st ECRS, Koshice, 2008, pp. 341–347.
[32] K. Maeda, J. Atmos. Terr. Phys. 19 (3–4) (1960) 184–245.
[33] S. Sagisaka, Nuovo Cim. C 9 (1986) 809–828.
[34] L.V. Volkova, Calculation of fluxes and angular distributions of high energy atmospheric muons at sea level, Preprint FIAN SSSR No. 72, Moscow, 1969 (in Russian).
[35] Particle Physics Booklet, 2008. Available from: <http://pdg.lbl.gov/>.
[36] D.E. Groom, N.V. Mokhov, S.I. Striganov, Muon stopping power and range tables 10 MeV–100 TeV, At. Data Nucl. Data Tables 78 (2001) 183–356.
[37] Yu.A. Glagolev, Reference Book on Physical Parameters of the Atmosphere, Gidrometeoizdat, Leningrad, 1970 (in Russian).
[38] Central Aerological Observatory (Russia, Dolgoprudny). Available from: <http://www.cao-rhms.ru/index.html>.
[39] B.C. Rastin, J. Phys. G: Nucl. Phys. 10 (1984) 1609–1628.
[40] O.C. Allkofer, K. Carstensen, W.D. Dau, Phys. Lett. B 36 (1971) 425–427.
[41] J. Kremer et al., Phys. Rev. Lett. 83 (1999) 4241–4244.
[42] P.Le. Coultre, L3+C Collaboration, Nucl. Phys. B (Proc. Suppl.) 145 (2005) 136–140.
[43] H. Jokisch et al., Phys. Rev. D 19 (1979) 1368–1372.
[44] O.C. Allkofer et al., Nucl. Phys. B 259 (1985) 1–18.
[45] S. Matsuno et al., Phys. Rev. D 29 (1984) 1–23.
[46] K. Murakami et al., Nuovo Cim. C 2 (5) (1979) 635–651.